ARMA 22–387

A case study on longwall-induced rockmass permeability under medium cover: Potential gas inflow implications

Khademian, Z.
CDC NIOSH, Pittsburgh Mining Research Division, Pittsburgh, PA, USA
Ajayi, K.M.
CDC NIOSH, Pittsburgh Mining Research Division, Pittsburgh, PA, USA
Kim, B.H.
CDC NIOSH, Spokane Mining Research Division, Spokane, WA, USA

This paper was prepared for presentation at the 56th US Rock Mechanics/Geomechanics Symposium held in Santa Fe, New Mexico, USA, 26-29 June 2022. This paper was selected for presentation at the symposium by an ARMA Technical Program Committee based on a technical and critical review of the paper by a minimum of two technical reviewers. The material, as presented, does not necessarily reflect any position of ARMA, its officers, or members. Electronic reproduction, distribution, or storage of any part of this paper for commercial purposes without the written consent of ARMA is prohibited. Permission to reproduce in print is restricted to an abstract of not more than 200 words; illustrations may not be copied. The

ABSTRACT: In the Northern Appalachian Basin of the United States, most of the production wells in shale gas reservoirs intersect with a bedded sequence of minable coal layers. The gas wells are often positioned in the coal mine abutment pillars for protection, but longwall-induced stresses may lead to excessive deformation in the gas well casing and potentially leak high-pressure gas to the mining area. Quantitative analyses of the potential gas inflow need an understanding of the rockmass permeability evolution during longwall mining. For this study, a medium-cover (198-m deep) mining site in eastern West Virginia was selected to calculate longwall mining-induced permeability changes. A model in 3DEC numerical modeling code was constructed using the Discrete Fracture Network (DFN) technique to explicitly create fracture systems in the model and calculate fracture apertures under longwall-induced stress and deformations. The calculated fracture apertures are used in a fracture flow code (FFC) to predict the volumetric gas inflow to the mine in the case of a hypothetical breach in a gas well casing. The potential breach location was identified using a 60-arm caliper survey in a test well in abutment pillar, showing that the maximum horizontal displacement occurs 51 m below the surface. The results of FFC simulation for the breach in this location shows that in 100 different DFN realizations, there is no sign of gas reaching the mine workings.

1. INTRODUCTION

Due to the specific geologic conditions in the Northern Appalachian Basin of the United States, many minable coal seams are located above shale gas reservoirs. Shale gas operation wells can intersect with future or active longwall mines, but guidelines must be followed to ensure the safety of both operations (PADEP 2018). If the longwall-induced deformation of rockmass surrounding the gas wells leads to excessive deformation and stress in well casings, the high-pressure, explosive gas may reach mine workings and overwhelm the mine ventilation systems. In order to protect gas wells from longwall-induced deformations, the wells are usually designed to be installed within the abutment pillars between longwall panels. However, for developing safety guidelines, it is important to quantify the amount of gas that would travel to the mine workings in case of well damage.

One of the critical parameters in quantifying gas inflow is the permeability of rockmass surrounding the gas well. Khademian et al. (2021) developed a geomechanical modeling methodology for estimating rockmass permeability changes due to longwall mining. This approach was based on the DFN technique for explicitly modeling fractures in rock (ITASCA 2022) and calculating their apertures affected by longwall stress and deformations. A shallow, 145-m-cover mine in the Pittsburgh coal seam was studied to calibrate DFN mechanical and hydraulic properties using pre-mining permeability measurements, and post-mining pillar stress and surface subsidence. The calibrated properties included: fracture friction coefficients being 60% of the strata internal friction, initial fracture apertures of 0.3–0.5 mm, fracture density (total fracture area in unit volume of rock) of 0.15 in weak coal horizon, fracture density of 0.2 for the shallow weathered zone, and fracture density of 0.3 for the interconnected fracture zone (with a height of about 23 times the mining height). After validating the models against post-mining permeability measurements, the fracture geometries and their apertures were used in a stochastic flow model to calculate potential gas inflow to the mine. Results showed that on average the potential inflow to the mine for an operating gas well pressure of 2.4 MPa for a hypothetical gas well breach at the Sewickley coal bed horizon, 23 m above the coal seam, was 0.22 m^3/s. The assumption of a potential Sewickley breach in the study site was based on an earlier work on potential planes of weakness with maximum longwall-

induced horizontal displacement (Zhang, Dougherty, et al. 2020).

In another case study (Khademian, et al. 2022), the same calibration parameters were used in a deep-cover (341 m) longwall mine in southwestern Pennsylvania in the Pittsburgh coal bed. The modeled permeability results were shown to agree reasonably with the field permeability measurements. The inflow rate was calculated for hypothetical damage to the well, 32 m above the mine roof. The results showed that, on average, the potential inflow to the mine level would be 0.006 m^3/s, about two orders of magnitude lower than the shallow-cover case value.

In this paper, an intermediate-cover (198-m) longwall in eastern West Virginia was selected to investigate the effects of cover depth on the inflow rate to the mine. This paper also employs the same methodologies and calibration properties for calculating the permeability. A 60-arm caliper logging was conducted for this work in a test well in the proximity of the gas wells to measure the longwall-induced horizontal deformation. The caliper logging showed the location of maximum deformation in the casing. Pillar stress was also measured by four borehole pressure cells (BPCs) placed horizontally into the test well abutment pillar. Detailed discussion on the caliper results and PBC measurements are provided by Zhang et al. (2022). After evaluating the model mechanical response, the fracture apertures were used to calculate the gas volumetric flow rate to the mine in the case of a hypothetical well casing breach at the location of the maximum casing deformation detected by the caliper survey.

2. DESCRIPTION OF MINE SITE AND IN-SITU MEASUREMENTS

A longwall mine under 198-m cover in eastern West Virginia is selected for this study. The overburden geology over the test site is a typical Pittsburgh seam geology and is highlighted by many strong and weak rock interfaces along weak layers. The longwall panel is 365-m wide with a mining height of 2.1 m.

The gas well is in a 31.6-m by 78.7-m abutment pillar that is part of a three-entry gateroad system between two longwall panels referred to as the second and third panels in this paper (Figure 1). The surface is not flat and the depth of cover ranges from 142 to 198 m. The rock types in the overburden are shale, sandstone, limestone, and coal with the field-scale geomechanical properties listed in

Table 1 (Zhang, Su and Dougherty, et al. 2020).

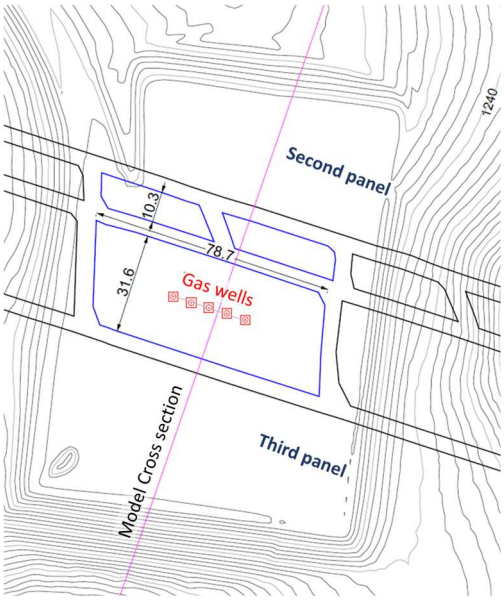

Figure 1. Gateroad entry layout in the location of the gas wells.

Table 1. Geomechanical properties applied to the model for each lithology

Rock Type	E	ν	C	Φ	T
Coal	2.1	0.3	1.9	28	0.3
Shale	11.6	0.25	11.7	35	4.5
Sandstone	11.6	0.22	17.9	35	6.9
Limestone	17.4	0.25	15.9	35	6.1

E: Elastic modulus (GPa), ν: Poisson's ratio, C: Cohesion (MPa), Φ: internal friction angle (degree), T: Tensile strength (MPa)

For detecting the location of maximum deformation in a casing due to longwall mining, a test well was drilled around the center of an abutment pillar close to the gas well abutment pillar but with a 186 m depth of cover, 12 m shallower than the gas well pillar. The test well was drilled to a depth of 207 m, about 30 m below the Pittsburgh seam. The test well casing was surveyed with a 60-arm caliper as the panel on either side mined by the test site for about 300 m (Zhang et al. 2022). The results in Figure 2 showed that the largest casing deformation with a diameter change of 8.2 cm occurred 51 m below the surface. This location is used as the potential breach location in the gas well for the calculation of volumetric gas flow to the mine later in this paper.

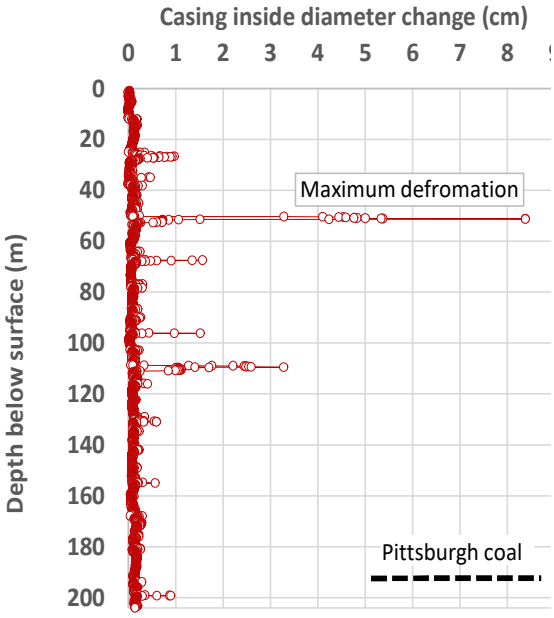

Figure 2. Casing diameter change measured by the 60-arm caliper survey after mining panels on either side of the test well.

In order to measure pillar stress variations, four borehole pressure cells (BPCs) 6 m apart were placed horizontally 8 m into the test well abutment pillar. BPCs showed that the pillar stress increases by 4 MPa after the first panel mined by the test well. Detailed discussion on the caliper results and PBC measurements are provided by Zhang et al. (2022).

3. GEOMECHANICAL MODEL

A three-dimensional distinct element code, 3DEC, is used for constructing a pseudo-2D longwall model (Figure 3) with one-meter length in the out-of-plane direction. In-situ stress with k=3 is applied in x direction and with k=2 in y direction. Displacement is fixed in y direction. Fractures in rock are explicitly modeled by DFN technique because rockmass permeability is mainly controlled by the permeability of its fracture systems.

3.1. Model geometry

From the core log data, geologic layers with a thickness less than 0.6 m are combined, and 55 bedding planes are modeled (Figure 3). A three-panel model is constructed with a length extended in the x direction, totaling 9,200 m to avoid significant boundary effects. The gas well is located between the second and third panels, but the effects of the first panel on the second panel need to be considered for realistic representation of longwall stresses around the abutment pillar.

DFN implementation for modeling fractured rock requires constraining site-specific fracture geometries and frictional properties that best represent rockmass mechanical and hydraulic behaviors under stress. Field observation of longwall-induced fracture orientations shows the propagation of subvertical fractures perpendicular to the mining face (Van Dyke et al. 2022). From field observations in Southwest Pennsylvania (Kohl 1980), the variation of the subvertical fracture dip angles is approximated to be 15° from 0–10 m above the mine roof, 12° from 10–30 m, 10° from 30–60 m, and 5° for the rest of the domain. The length of fractures is assumed limited to the thickness of the strata with a negative power law distribution with a scaling exponent of 1.1. Uniform distribution is used for the fracture position within each individual lithology (Feng 2018).

The fracture density, or P32 value, is the total fracture surface in unit volume. Fracture mapping was not conducted in this mining site, so the values are inferred from the previous study on a shallow Pittsburgh coal longwall site (Khademian, et al. 2021) where fracture densities were limited to a 0.1 to 0.3 m^2/m^3 range with higher densities applied to weaker zones. Here, the weak zones include the shallow weathered zone, Waynesburg

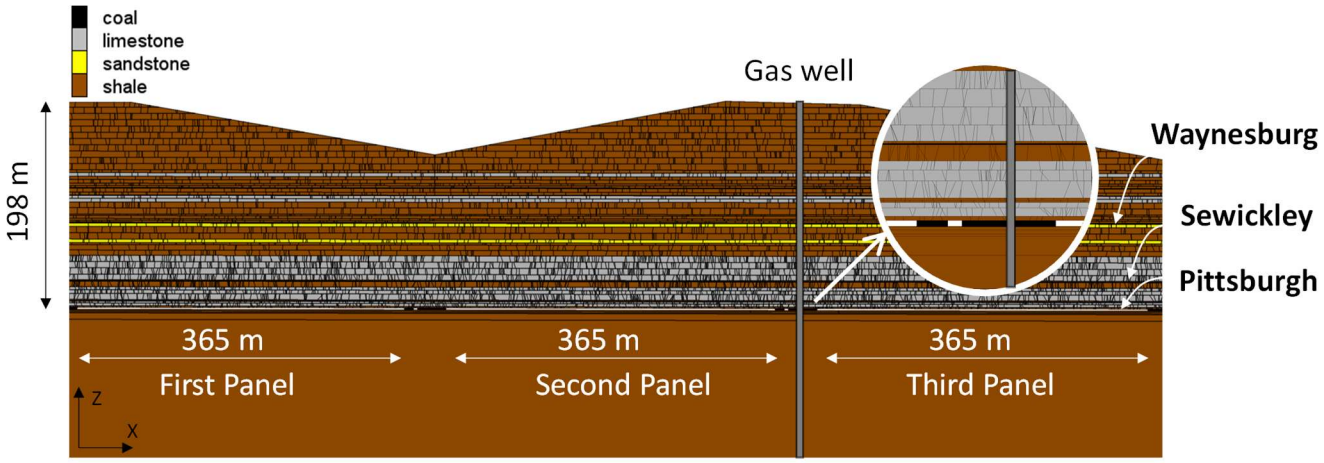

Figure 3. Details of the central part of the 3DEC model of a medium-cover longwall mine with DFN defining rockmass structures in 55 modeled lithologies.

horizon, Sewickley horizon, and an interconnected longwall-induced fracture zone (Figure 4). As defined by Palchik (2003), the combined thickness of the caved area and the lower part of the fractured zone above it are considered an interconnected fracture zone representing a system of channels that are hydraulically connected and allow for flow transport to the mine level. Palchik (2003) estimated the thickness of this zone to be 19–43 times the mining height following a set of field measurements. Khademian et al. (2021) reproduced reasonable rockmass permeability and pillar stresses by assuming an interconnected fracture zone with a height 23 times the mining height. It was also shown that reasonable surface subsidence and pillar stress can be obtained by assigning the friction of subvertical DFN fractures and bedding planes with 60% of the internal friction of rock in each layer, except for the fractures in the interconnected fracture zone that are assigned a constant friction angle of 10 degrees.

For modeling permeability of rockmass, the fracture apertures are calculated in 3DEC with the variation of longwall stresses. However, when constructing the pre-mining model, an initial aperture value must be assigned to the fractures before applying in-situ stresses. Khademian et al. (2021) obtained reasonable pre-mining and post-mining permeabilities by assigning an initial aperture of 0.4 to 0.5 mm for both bedding planes and subvertical fractures. So, here an initial aperture of 0.4 mm is assigned to the fractures before initializing in-situ stress in the model.

3.2. Gob model

Compaction of residual void spaces in the longwall gob affects the induced stresses and deformations of surrounding rockmass (Pappas and Mark 1993) and thus can affect the aperture of fracture systems. Deformations due to the compaction of the gob are accounted for by installing a gob model at the roof of the panels. Pappas and Mark (1993) showed that the stress-strain response of caved material should follow a hyperbolic strain-hardening curve defined by Salamon (1990):

$$\sigma = \frac{a \times \varepsilon}{b - \varepsilon} \qquad (1)$$

where σ is vertical gob stress (MPa), ε is vertical gob strain, b is the maximum strain parameter related to the void ratio, and a is the gob stress where $\varepsilon = b/2$ (MPa).

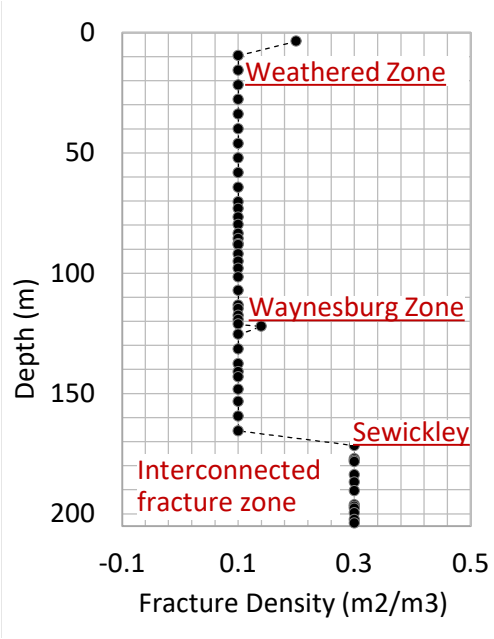

Figure 4. DFN densities in each layer along the overburden used to generate subvertical fractures.

Esterhuizen, Mark and Murphy (2010) simulated the gob in FLAC3D with an equivalent element method, but this treatment of gob effects in 3DEC may lead to excessive overlap of blocks. Khademian et al. (2022) simulated gob effects in 3DEC by applying counteracting loads onto the mine roof accounting for both gradual development of panels and gob effects. The red dashed curve in Figure 5 shows the average of the excavation-relaxing stresses applied onto the roof after mining the third panel in the model. At the same time, gob effects are modeled by applying incremental stresses at the same boundaries based on Equation 1 with a=3 MPa and the assumption of a maximum strain of 44%. The average of the gob-simulating stresses is shown as a solid black curve in Figure 5.

Once the model reaches equilibrium, the surface subsidence and pillar stresses are recorded. Figure 6 shows the supercritical surface subsidence recorded in the model with a maximum value of 1.44 m about 67% of the mining height, which is expected from a supercritical longwall panel.

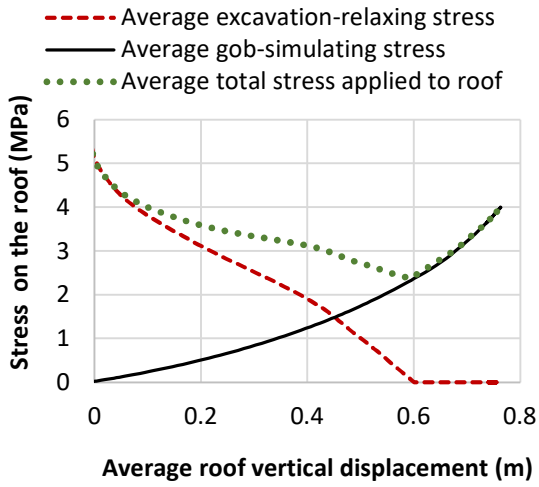

Figure 5. Boundary loads applied to the mine roof in the 3DEC model.

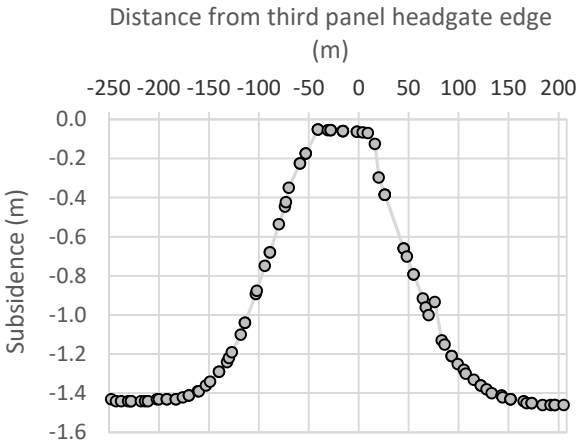

Figure 6. Surface subsidence calculated in the 3DEC model with a maximum subsidence of 1.44 m.

Figure 7a and 7b show the vertical stress in the pillar after the second and third panels are completely developed in the model, respectively. The in-situ vertical stress at the mine level is about 5 MPa. After mining the second panel, the **average** vertical stress at the abutment pillar increases to about 8 MPa from the virgin stress. The measured stress by the BPCs is also plotted in Figure 7a, showing a vertical stress increase of 4 MPa at the measurement location, confirming the model response at this location. Mining the third panel increases the **average** vertical stress to 16 MPa. As shown in Figure 7, the gob stress after mining each panel gradually approaches the in-situ stress level of 5 MPa, which reflects the expected gob effects after mining the panels.

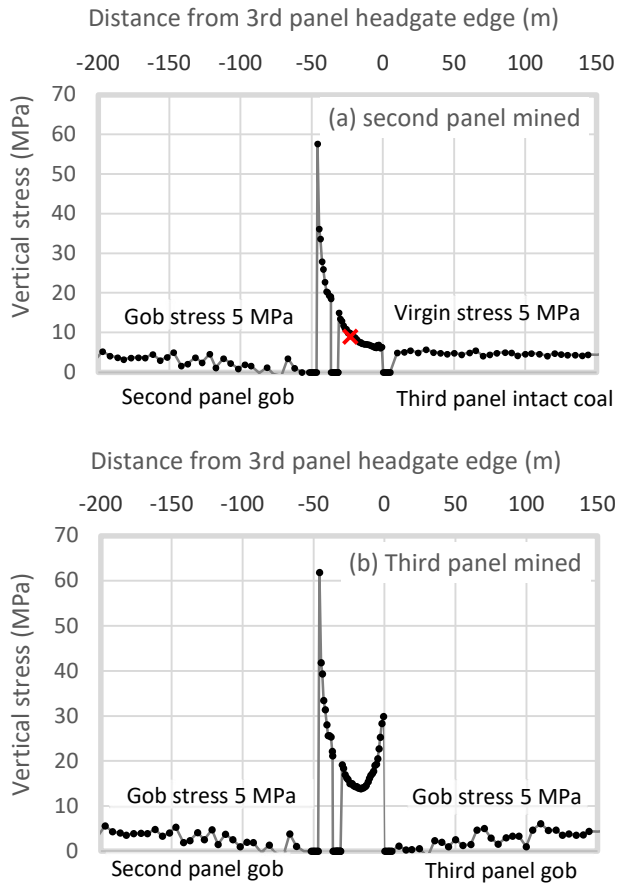

Figure 7. Modeled pillar vertical stress (a) after mining the second panel and (b) after mining the third panel.

3.3. Aperture variation

Apertures of subvertical fractures and bedding planes are recorded before and after loading the model and then after the development of each panel. Figure 8a and Figure 8b show the aperture values above the abutment pillar where the gas well is located. All fractures are initialized with an aperture of 0.4 mm before initializing in-situ stresses. The range of apertures expand from 0.4 mm to 0.01 and 5 mm due to the pre-mining stresses. The first panel development affects the aperture values in the abutment pillar between the second and third panels. This range further expands as mining continues in the second and third panels.

The widening of the aperture ranges after developing each panel shows how mining-induced stresses can both increase and decrease fracture apertures in different locations above the abutment pillar. The vertical loads transferred to the pillar compact the bedding planes at the central part of the pillar. However, deformation caused by the roof caving at the pillar edges increases the aperture

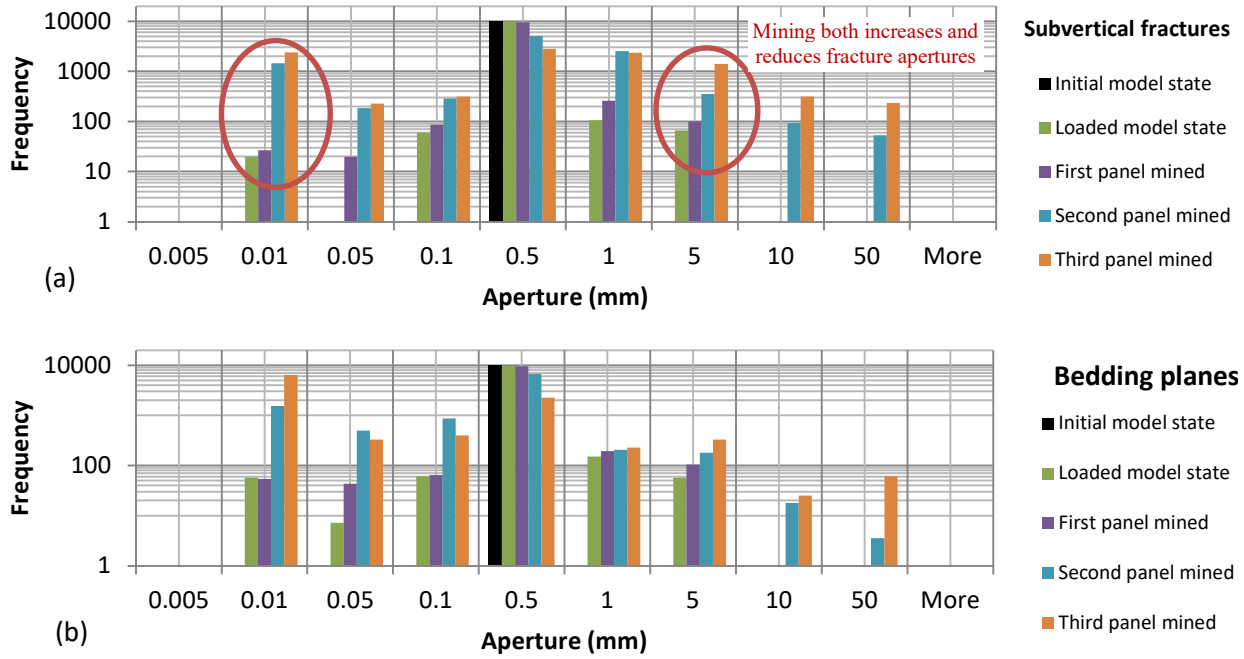

Figure 8. Aperture variations under different loadings for (a) subvertical fractures and (b) bedding planes.

of bedding planes while opening subvertical fractures in the central part of the pillar.

3.4. Permeability calculation

Based on the calculated aperture values, permeabilities of subvertical fractures and bedding planes can be calculated at each layer in the model. It is assumed that rock matrix permeability is zero and gas can only flow through the fracture networks.

Permeabilities are calculated following the approach explained by Khademian et al. (2021) based on the Cubic Law and Darcy's equation. For each layer from the surface down to the 198-m level, permeabilities are obtained in an area above the abutment pillar between the second and third panels. This area provides an understanding of permeability values around the potential gas well location. Figure 9 demonstrates the modeled permeabilities showing that subvertical fracture permeabilities are in general less than the bedding plane permeabilities at shallow depths. This is mainly due to the high-horizontal stress to vertical stress ratio (k = 3) and the surface subsidence affecting beds' integrity. Approaching the mine level, the loads transferred to the pillar area from the retreated panels compacts the bedding planes and reduces their permeabilities down to the subvertical permeability level. Permeabilities of both fracture groups increase by several orders of magnitude within 40 m from the mine level. The quantity of gas traveling from a hypothetical breach in the gas well to the mine level depends on the overall permeabilities of subvertical fracture and bedding planes, so a fracture flow code (FFC) is used for estimating the quantity of the gas flow rate to the mining area.

4. INFLOW ESTIMATION

As discussed in the Introduction, the apertures predicted from 3DEC are used to predict the potential gas flow to the mine in the event of a hypothetical casing breach. The apertures are imported into the fracture flow code (FFC) using the methodology presented by Ajayi et al. (2021). The code generates a stochastic DFN model using power law distributions for fracture length, Von-Mises Fisher's distribution for fracture orientation, and uniform distribution for fracture location. A multizone approach is incorporated to import the exact aperture values from the 3DEC geomechanical model to FFC. The impact of a hypothetical breach is investigated at a depth of 51 m from surface, which is predicted as the potential casing breach horizon for this specific site.

A gas well operating pressure of 2.4 MPa is defined at the breach location and the pressure at the other locations are set to zero, except the mine roof, where a negative pressure is defined to represent the mine ventilation system. The fractures are assumed to be 25% saturated with immobile water (Ajayi, et al. 2021). The shale gas is modeled as methane, and 100 DFN realizations are generated to represent multiple variations in the fracture geometry. Even though there could be several wells on a well pad, this study focuses on a single casing breach 51 m below the surface. One-hundred stochastic DFN realizations are generated to model variation in the fracture geometry, connectivity, and aperture. The results show that there is no flow to the mine in any of the 100 realizations. However, an average gas flow rate of 0.00045 m3/s was observed at the surface. This observation is unique to this site because the potential

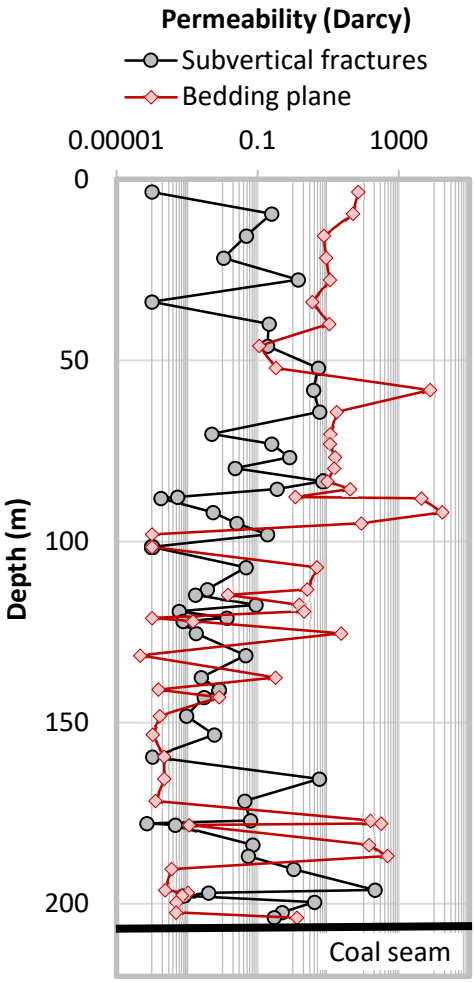

Figure 9. Results of modeled permeability above the abutment pillar along the depth when the second panel is outby the test site.

breach location (51 m below surface) is significantly closer to the surface than the mine at a depth of 198 m.

5. DISCUSSION

So far, in this series of papers, three mine sites with shallow, intermediate, and deep covers were studied. The same methodology and calibrated fracture properties are followed for the calculation of permeability changes due to longwall mining. The gas volumetric flow rate is calculated for each case. The shallow-cover case (147 m) yielded a flow rate of 0.22 m^3/s for the gas well operating pressure of 2.4 MPa applied at the Sewickley level, 23 m above the roof where the maximum horizontal displacement occurs (Khademian, et al. 2021). The flow rate for the deep-cover case (341 m) was 0.006 m^3/s for a breach at the Sewickley level (32 m above roof) with 2.4 MPa gas pressure (Khademian, et al. 2022). This paper shows that for a medium-cover case (198 m), the flow rate value for the same gas pressure at the location of the maximum horizontal displacement (51 m below surface) is zero. Further investigation is needed to quantify the effects of overburden and geology on the permeability evolution of rockmass due to longwall mining.

It is important to note that the fracture properties in the current model are borrowed from the shallower-cover site with the overburden depth of 147 m, which can be a source of uncertainty. This is because the fracture geometries (density and orientation) along with the fracture mechanical and hydraulic properties can be site specific, depending on the depth of cover, mining layout, and overburden geology. Having said that, studying the three mine sites showed that the geomechanical model under these assumptions reproduced the expected or measured surface subsidence, pillar stress, and gob stresses. Also, the modeled permeabilities for the shallow- and deep-cover cases were shown to agree with the field measurements. However, further analyses are required to test the applicability of the developed approach for different mine layouts, lithology, and depths of cover.

6. CONCLUSION

This paper discusses the application of a modeling methodology previously developed by researchers at the National Institute for Occupational Safety and Health (NIOSH) for calculating the rockmass permeability induced by mining the Pittsburgh coal seam under 198-m cover. The potential inflow to the mining area in case of a breached gas well in the abutment pillar is calculated. The mechanical response of the model, including surface subsidence, pillar stress, and gob material stresses is shown within the expected range in similar mining conditions. Fracture apertures across the models are calculated and exported to the FFC models. The FFC model calculates the volumetric gas inflow based on a gas well operating pressure of 2.4 MPa at a hypothetical breach location in the gas well 51 m below the surface. In 100 simulations with different DFN realizations, no sign of gas inflow to the mine was recorded. Comparing the results with previous studies in this series of papers on a 147-m-deep mining case (0.22 m^3/s inflow for a breach at 23 m above roof) and a 341-m-deep mining case (0.006 m^3/s for a breach at 32 m above roof) implies a dependence of gas inflow on the depth of cover and the potential breach location. More case studies with different overburden geology and mine layouts will be investigated in this series of papers to quantify potential gas inflow ranges under different conditions. The results can be used for studying shale gas well design and mine ventilation requirements where gas wells intersect with longwall mines.

7. DISCLAIMER

The findings and conclusions in this paper are those of the authors and do not necessarily represent the official

position of the National Institute for Occupational Safety and Health (NIOSH), Centers for Disease Control and Prevention.

8. REFERENCES

1. Ajayi, Kayode, Zoheir Khademian, Steven J Schatzel, Eric A Watkins, and Vasu Gangrade. 2021. "Numerical Modeling of Longwall-induced Permeability under shallow cover." 18th North American Mine Ventilation Symposium. Rapid City, SD.
2. Esterhuizen, G. S., C Mark, and M. M. Murphy. 2010. "Numerical Model Calibration for Simulating Coal Pillars, Gob and Overburden Response." 29th International Conference on Ground Control in Mining. Morgantown, WV: Barczak T, ed. 46-57.
3. Feng, et al. 2018. "Distribution of gob empty space for methane drainage during the longwall mining: A case study." Journal of Natural Gas Science and Engineering 112-124.
4. ITASCA. 2022. "3DEC 7.0 documentation."
5. Khademian, Z, A. M. Kayode, D. W. H. Su, S. J. Schatzel, B. H. Kim, and G. S. Esterhuizen. 2022. "Rockmass permeability induced by longwall mining under deep cover: potential gas inflow from a sheared gas well." SME annual conference. Salt Lake City.
6. Khademian, Z., K. M. Ajayi, D. W. H. Su, G. Esterhuizen, and S. J. Schatzel. 2021. "Geomechanical Modeling of Mining-Induced Permeability: Implications for Potential Gas Inflow from a Sheared Gas Well." 40th International Conference on Ground Control in Mining.
7. Kohl, W. R. . 1980. Jointing in outcropping rocks of Pennsylvanian age, central Greater Pittsburgh region, Pennsylvania. U.S. Geological Survey.
8. PADEP. 2018. 2018 Oil and Gas Annual Report. Pennsylvania Department of Environmental Protection.
9. Palchik, V. 2003. "Formation of fractured zones in overburden due to longwall mining." Environmental Geology 28-38.
10. Pappas, D.M., and C. Mark. 1993. Behavior of Simulated Gob Material. . U.S. Bureau of Mines RI 9458.
11. Salamon, M.D.G. 1990. "Mechanism of caving in longwall coal mining. ." 21th U.S. Rock Mechanics Symposium. Denver CO. 161-168.
12. Van Dyke, M., P. Zhang, H. Dougherty, D. W. H. Su, and B. H. Kim. 2022. "Identifying Longwall-Induced Fractures through Core Drilling." Annual Conference of Society of Mining, Minerals, and Exploration.
13. Zhang, P., D. W. H. Su, B. H. Kim, and E. Midler. 2022. "Comparison of casing deformations between measurements and numerical modeling of a test well in longwall chain pillars." 56th US Rock mechanics /Geomechanics Symposium. Santa Fe, New Mexico.
14. Zhang, P., D. W. H. Su, H. Dougherty, R. Kimutis, S. Schatzel, and J. Lu. 2020. "A Case Study on Longwall Mining near Shale Gas Wells in Barrier Pillars – Influence, Safety, and Risks." 54th US Rock Mechanics/Geomechanics Symposium. Golden.
15. Zhang, P., H. Dougherty, D. W. H. Su, J. Trackemas, and B. Tulu. 2020. "Influence of longwall mining on the stability of gas wells in chain pillars." International Journal of Mining Science and Technology.